Earth and Planetary Science Letters 498 (2018) 185–195

Contents lists available at ScienceDirect

Earth and Planetary Science Letters

www.elsevier.com/locate/epsl

# Ocean and climate response to North Atlantic seaway changes at the onset of long-term Eocene cooling

Maximilian Vahlenkamp [a,*], Igor Niezgodzki [b,c], David De Vleeschouwer [a], Gerrit Lohmann [b], Torsten Bickert [a], Heiko Pälike [a]

[a] MARUM – Center for Marine Environmental Sciences, University of Bremen, Leobener Strasse 8, 28359 Bremen, Germany
[b] Alfred Wegener Institute Helmholtz Centre for Polar and Marine Research, Bussestr. 24, 27570 Bremerhaven, Germany
[c] ING PAN – Institute of Geological Sciences, Polish Academy of Sciences, Research Center in Kraków, Biogeosystem Modelling Laboratory, Kraków, Poland

ARTICLE INFO

*Article history:*
Received 24 October 2017
Received in revised form 12 June 2018
Accepted 17 June 2018
Available online xxxx
Editor: M. Frank

*Keywords:*
Northern Component Water
Earth System Model
Greenland–Scotland Ridge
Deep Western Boundary Currents
Eocene cooling

ABSTRACT

Around the early–middle Eocene boundary, the first occurrence of contourite drift sediments and widespread deep ocean erosion indicate changes in the North Atlantic ocean circulation. Interestingly, these changes coincide with the first steps of Cenozoic cooling from the Paleogene greenhouse climate towards the modern icehouse. The cause for this ocean circulation reorganization is poorly understood since modern water mass tracers may have worked fundamentally different in the past and the paleoceanographic proxy record is limited in both time and space. As a result, it is challenging to reliably reconstruct the climatic and tectonic boundary conditions e.g. atmospheric greenhouse gas concentration and the depth and geometry of developing and closing passages between ocean basins. In this study, we attempt to identify thresholds in tectonic gateway passages and atmospheric $CO_2$ concentration, using the fully coupled Earth System Model *COSMOS*. Indeed, the simulation of Earth's past climates can unravel the physical processes driving deep-water formation in a greenhouse world. Specifically, we use COSMOS to evaluate the impact of changes in the North Atlantic gateways at the early–middle Eocene boundary on the North Atlantic Deep Western Boundary Currents under low obliquity configuration. We find that Northern Component Waters start to form when the Greenland Scotland Ridge reaches a threshold depth of deeper than 200 m, while the Arctic Ocean is still shut off from the North Atlantic. In this scenario, the relatively deep Greenland Scotland Ridge allows for sufficient inflow of warm, salty Atlantic surface waters into the Nordic Seas to initiate convection during winter cooling. Opening the seaway towards the Arctic leads to a cessation of Northern Component Water formation as it allows for inflow of brackish surface waters into the northern Nordic Seas, hindering Northern Component Water formation.



## 1. Introduction

Large-scale climate change over the course of the Cenozoic has been linked to changes in ocean gateway configurations and their respective impact on the global ocean circulation (e.g. Berggren, 1982; Berggren and Hollister, 1977; Kennett, 1977). One of the challenges of modeling past ocean circulation and climate arises from the large uncertainties in boundary conditions throughout the geologic past. The sedimentary record of the early–middle Eocene, for example, is more fragmented in both time and space compared to younger time slices of the Cenozoic. Hence, while uncertainties of Eocene GHG (greenhouse gas) concentration estimates have lately declined (Anagnostou et al., 2016), paleogeography and paleobathymetry remain poorly constrained throughout this epoch. Important uncertainties in Eocene paleobathymetry reside in the depth of important seaways in the North and South Atlantic.

During the Eocene, a number of paleogeographic changes could have led to the onset of the meridional deep-water circulation with a deep-water source in the North Atlantic: (i) The Nordic Seas widened considerably during the early Eocene but were still separated from the Atlantic by the Greenland–Scotland Ridge (GSR) (e.g. Mosar et al., 2002). The long-term subsidence of the GSR has been superimposed by Icelandic mantle plume activity with reoccurring intervals of uplift and sinking. However, mantle plume activity decreased during the late early Eocene (Parnell-Turner et al., 2014) and a first marine connection between the North Atlantic and the Nordic Seas is indicated by similar planktonic microfauna and microflora on either side of the GSR (Berggren and Schnitker, 1983; Hulsbos et al., 1989). While some parts of the GSR may still have been above sea level during the early–middle Eocene, a num-

* Corresponding author.
*E-mail address:* mvahlenkamp@marum.de (M. Vahlenkamp).

https://doi.org/10.1016/j.epsl.2018.06.031

ber of deep gateways bisecting the GSR, such as the Faroe–Shetland Channel have already allowed for substantial overflow (Hohbein et al., 2012; Thiede and Eldholm, 1983). The initiation of a stable, southwest deep-water overflow from the Faroe–Shetland basin into the North Atlantic from ca. 49 Ma onwards over this part of the GSR is attested by the Judd Fall Drifts, deposited at the southwest end of the Faroe–Shetland Basin (Hohbein et al., 2012).

(ii) In the northern high latitudes, the Arctic Ocean was a largely landlocked basin from its formation in the early Cretaceous to the early Eocene, even though during that time limited, periodic shallow water connections to the global oceans existed (Jakobsson et al., 2007). At the end of the early Eocene however, low sea surface salinities in the Arctic Ocean support progressing restriction of oceanic exchange between the Arctic Ocean and adjacent seas (Brinkhuis et al., 2006) and the cessation of the connection between the Arctic Ocean and the Tethys through the Turgai Strait (Gleason et al., 2009). The low sea surface salinity (SSS) in a completely landlocked Arctic Ocean would be compensated by a positive SSS anomaly in the North Atlantic, potentially affecting global oceanic circulation (Roberts et al., 2009). However, periodic exchange between the Arctic Ocean and the Nordic Seas through a narrow and shallow seaway has likely existed from ∼45 Ma onwards (Onodera et al., 2008).

(iii) During the middle Eocene, the Tethys Ocean continued its separation into the Neo-Tethys in the East and the Alpine Tethys in the West with only shallow shelf connections between the two basins (Schettino and Turco, 2011). The depth and flow capacity of the seaway between Africa in the South and Iberia in the North are poorly constrained, yet the seaway became successively more restricted during the Eocene (Ziegler, 1988). Plate reconstructions range from a very narrow, shallow water connection to a deep-water connection allowing for large-scale exchange of deep water (Schettino and Turco, 2011; Stampfli and Hochard, 2009).

(iv) In the Southern Ocean, the opening of the Tasman and Drake Passages enabled due to the separation of Australia and South America from Antarctica led to the initiation of the Antarctic Circumpolar Current (ACC) and has been invoked as the trigger of Eocene cooling and the glaciation of Antarctica (e.g. Berggren and Hollister, 1977; Bijl et al., 2013; Kennett, 1977). The opening of the Drake Passage is of complex nature as reflected by widely separated estimates of the timing of Drake Passage throughflow, which range between ∼50 (Livermore et al., 2005) and ∼17 Ma (Barker, 2001). More recent estimates based on Neodymium (Nd) isotopes report considerable inflow from the Pacific to the South Atlantic through the Drake Passage since the late middle Eocene at the latest (Livermore et al., 2007; Scher and Martin, 2006). The (deep-)opening of the Tasman Passage has been dated close to the Eocene–Oligocene boundary (Stickley et al., 2004) and linked to the initiation of the (proto-)ACC to the major glaciation of Antarctica at this time (e.g. Kennett, 1977). However, a shallow opening of the Tasman Passage likely occurred already near the early–middle Eocene boundary (Bijl et al., 2013; Exon et al., 2002) and progressively deepened up to 2000 m depth just after the Eocene–Oligocene boundary (Lawver and Gahagan, 2003).

Cenozoic GHG concentrations peaked during the Early Eocene Climatic Optimum (52–50 Ma). Estimates for the early and middle Eocene atmospheric $CO_2$ concentrations range from 680–1260 ppm (Anagnostou et al., 2016; Franks et al., 2014; Jagniecki et al., 2015) and global deep ocean temperatures were up to 12 °C higher than today (Zachos et al., 2001). Latitudinal temperature gradients are reported to be less steep compared to today (e.g. Fricke and Wing, 2004; Greenwood and Wing, 1995; Zachos et al., 1994) and continental ice was largely absent or ephemeral (e.g. Miller et al., 1987, 2005b). The middle Eocene marks the beginning of the transition from the early Eocene warmhouse towards the cooler Oligocene climate. From approximately 49 Ma onwards, temperatures gradually decreased, related to a reduction in atmospheric $CO_2$ by as much as 400 ppm (Anagnostou et al., 2016) due to declining volcanic $CO_2$ emissions (Zachos et al., 2008) as well as to the burial of vast amounts of organic carbon during the so-called 1.2 Myr long *Azolla* phase in the Arctic Ocean (Brinkhuis et al., 2006). The deposition of this fast growing freshwater fern in parts of the Arctic Ocean, the Nordic Seas and the North Atlantic would have removed an estimated 55–470 ppm of $CO_2$ from the atmosphere at the onset of Cenozoic cooling (Backman et al., 2006; Barke et al., 2012; Speelman et al., 2009). Finally, the above-mentioned tectonic events played a crucial role in the long-term climate cooling during the middle Eocene by reshaping inter-basinal exchange and the global ocean circulation. The onset of global cooling around 49 Ma coincides with major changes in deep-ocean circulation as evident through changes in the global inter-basinal gradient (Sexton et al., 2006), warming of the Atlantic relative to Pacific deep waters (Cramer et al., 2009) and enhanced global productivity (Nielsen et al., 2009). The cooling increased the meridional temperature gradients and reduced the previously high precipitation in high latitudes (Speelman et al., 2010; Wing, 2003).

In the early Cenozoic, deep-water formation occurred primarily in the Southern Ocean (Mountain and Miller, 1992; Pak and Miller, 1992; Thomas et al., 2003), whereas by the middle Eocene bottom water source areas in the Atlantic may have periodically shifted (Oberhänsli et al., 1991). Conflicting ocean circulation proxy results from only a few deep-ocean sites around the globe, and modeling studies have led to a vigorous discussion about the timing of the onset of the modern-style bimodal regime with deep-water formation in the North Atlantic and the Southern Ocean. The most compelling evidence for the onset of Northern Component Water (NCW) at the early–middle Eocene boundary comes from North Atlantic Drift sediments, which are deposited under the influence of bottom currents such as the Deep Western Boundary Currents (DWBC) associated with an invigoration of the Atlantic Meridional Overturning Circulation (AMOC). Davies et al. (2001) proposed an onset of NCW at 35 Ma based on the identification and dating of the, at that time, oldest known North Atlantic Drift Sediments. More recently, Hohbein et al. (2012) re-dated the onset of NCW to 49 Ma based on the onset of sediment drift deposits within a restricted sedimentary basin at the GSR, a key gateway for modern North Atlantic Deepwater (NADW) outflow into the North Atlantic. This age close to the early–middle Eocene boundary is supported by the onset of the Newfoundland Drifts shortly afterwards (Boyle et al., 2017) in the pathway of the DWBC.

Nd isotopes are used to track changes in ocean circulation as they are imprinted with the Nd isotope signature of their source regions. Nd isotopes from the South Atlantic and the Southern Ocean have been interpreted to indicate the onset of NCW close to the Eocene–Oligocene boundary (Via and Thomas, 2006), even though it was noted that a less radiogenic water-mass (either NCW or Warm Saline Deep-Water (WSDW) from the Tethys) must have been present in the South Atlantic during the middle Eocene (Scher and Martin, 2004). More importantly, unradiogenic Nd isotopes (characteristic of modern NADW) from the late Eocene Labrador Sea indicate that the Southern Ocean was not the source of bottom waters at this time, but that NCW already filled parts of the North Atlantic by the late Eocene (Coxall et al., 2018).

On the other hand, relatively high values of benthic foraminiferal $\delta^{13}C$ reflect a dominance of a nutrient-enriched deep-water source (as characteristic of modern southern-sourced bottom waters) during the middle Eocene. Curiously, during the Eocene and Oligocene the phase relationship between Nd isotopes and $\delta^{13}C$ in the South Atlantic is inversed compared to the modern, with most unradiogenic values corresponding to low $\delta^{13}C$ (Scher and Martin, 2004). Two possible explanations for the inversed relationship be-

**Table 1**
Experimental setup.

| | *cntrl840* | *cntrl1000* | *GSR50* | *GSR200* | *ASO* | *TSO* |
|---|---|---|---|---|---|---|
| $CO_2$ [ppm] | 840 | 1000 | 840 | 840 | 840 | 840 |
| Greenland–Scotland Ridge [m] | 500 | 500 | 50 | 200 | 500 | 500 |
| Arctic seaway [m] | closed | closed | closed | closed | 200 | closed |
| Tethyan seaway [m] | closed | closed | closed | closed | closed | 1800 |
| Nordic Seas [m] | 500 | 500 | 500 | 500 | 500 | 500 |

tween Nd isotopes and benthic foraminiferal $\delta^{13}C$ are discussed. Firstly, initial NCW could have been more nutrient-rich than modern NADW (Coxall et al., 2018) due to the more isolated setting of the Nordic Seas. Alternatively, the carbon isotopic signature of bottom waters during the middle Eocene could have been driven by geographic differences in top-down productivity rather than bottom water ventilation in comparison with the modern ocean.

Other studies have utilized inter-basinal benthic foraminiferal $\delta^{18}O$ gradients to track the onset of the modern bimodal ocean circulation, suggesting the onset of NCW during the late middle Eocene at 38.5 Ma, not precluding however an earlier contribution of NCW from GSR overflow (Borrelli et al., 2014; Langton et al., 2016).

In the same way as paleoceanographic proxies, climate- and ocean circulation models disagree about the timing and mechanisms behind the onset of deep-water formation in the North Atlantic. Some studies obtain a bimodal AMOC under early Eocene boundary conditions (e.g. Huber and Sloan, 2001) while others invoke gateway changes during the later Cenozoic as the trigger of NCW formation. Recent studies link changes in the North Atlantic like the isolation of the Arctic Ocean (Roberts et al., 2009), the subsidence of the GSR (Stärz et al., 2017) or the cessation of the Tethyan Seaway (Zhang et al., 2011) to the onset of NCW. Others propose changes in the South Atlantic like the opening of the Tasman and Drake Passages and the formation of the ACC (Elsworth et al., 2017; Fyke et al., 2015) as the trigger for the onset of a bimodal deep-water formation. While some of the mentioned studies have already looked into the effects of gateway openings in the North Atlantic on ocean circulation (Roberts et al., 2009; Stärz et al., 2017; Zhang et al., 2011), all of them used continental setups with open Southern Ocean gateways allowing for the formation of a (proto-)ACC.

In this study, we use the fully coupled Earth System Model *COSMOS* to assess the sensitivity of Earth's climate system to changes in North Atlantic Ocean gateways under early–middle Eocene boundary conditions and thus before the initiation of the (proto-)ACC. In this way, we explore the role of the North vs. South Atlantic in the establishment of the modern ocean circulation and test the role of distinct tectonic events for the onset of NCW. It should be noted though, that while the modeled setups are plausible scenarios based on geological evidence, the exact paleodepth of the gateways are hard to pinpoint. Our simulations are designed to provide insight into the mechanisms responsible for the initiation of NCW and the invigoration of DWBCs at the early–middle Eocene boundary rather than to evaluate their exact amplitudes.

## 2. Model and experiment design

We use the Community Earth System Model (*COSMOS*) in the coupled atmosphere–ocean configuration with prescribed vegetation. The model setup includes the atmosphere component ECHAM5 at T31/L19 resolution, i.e. a horizontal resolution of ~3.75° with 19 vertical layers. A detailed description of the ECHAM5 model is given by Roeckner et al. (2003). The Max Planck Institute Ocean Model (MPI-OM) runs in a GR30/L40 configuration with an average horizontal resolution of 3° × 1.8° and 40 unevenly-spaced vertical layers (Marsland et al., 2003) and in-

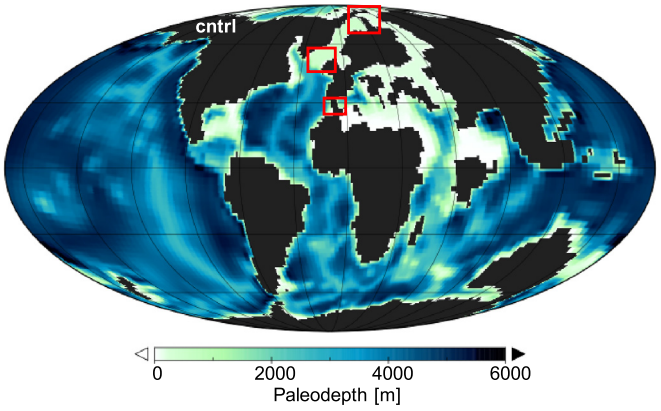


**Fig. 1. Global paleogeography of the early–middle Eocene** as used for the *cntrl840* and *cntrl1000* simulations. Gateway depths in the circled areas for the different experiments are given in Table 1 and shown in detail in Supplementary Figs. 1–3. (For interpretation of the colors in the figure(s), the reader is referred to the web version of this article.)

cludes a dynamic–thermodynamic sea ice model after (Hibler, 1979) that simulates the distribution and thickness of sea ice considering surrounding climatic conditions, while overturning by convection is implemented via increased vertical diffusion (Jungclaus et al., 2006). The boundary conditions to run the model include the prescription of vegetation distribution (Sewall et al., 2007), the set-up of the hydrological discharge model (Hagemann and Dümenil, 1997), orography-related parameters for the gravity wave drag parameterization (Lott and Miller, 1997), glacier mask, the concentration of the greenhouse gases in the atmosphere and orbital parameters. The solar constant was reduced by 0.6% compared to present-day and equals 1358.8 $W/m^2$ (Gough, 1981). Preindustrial control runs as well as future climate warming scenarios of the fully coupled COSMOS model in the configuration and resolution used in this study have been published by Knorr et al. (2011) and Gierz et al. (2015).

Early–middle Eocene boundary conditions in our control simulation were specified by using a paleogeography representative for the Ypresian (56–47.8 Ma) compiled by GETECH paleogeography (Lunt et al., 2016) with the following modifications: (i) opening the connection between the Nordic Seas and the North Atlantic at the GSR to account for the changes close to the early–middle Eocene boundary (Hohbein et al., 2012), (ii) restricting the connection between the Tethyan Ocean and the Atlantic Ocean (Stampfli and Borel, 2004) and (iii) opening the Turgai Strait to the Arctic because COSMOS does not support enclosed seas. No ice sheets were prescribed in either hemisphere. We use present-day values for eccentricity and precession, and a low value of 22.1° for obliquity, as such astronomical configuration favors NCW formation (Vahlenkamp et al., 2018).

All simulations are run with 3 x pre-industrial $CO_2$ level (840 ppm) (Anagnostou et al., 2016), except *cntrl1000* which was set to 1000 ppm. Concentrations of other greenhouse gases were set to present day values. The experimental setup, including modifications to the oceans' bathymetry, is provided in Table 1 and Fig. 1.

Our *cntrl840* simulation was run for 7700 years. All other experiments were restarted from the *cntrl840* at year 6200 and sim-

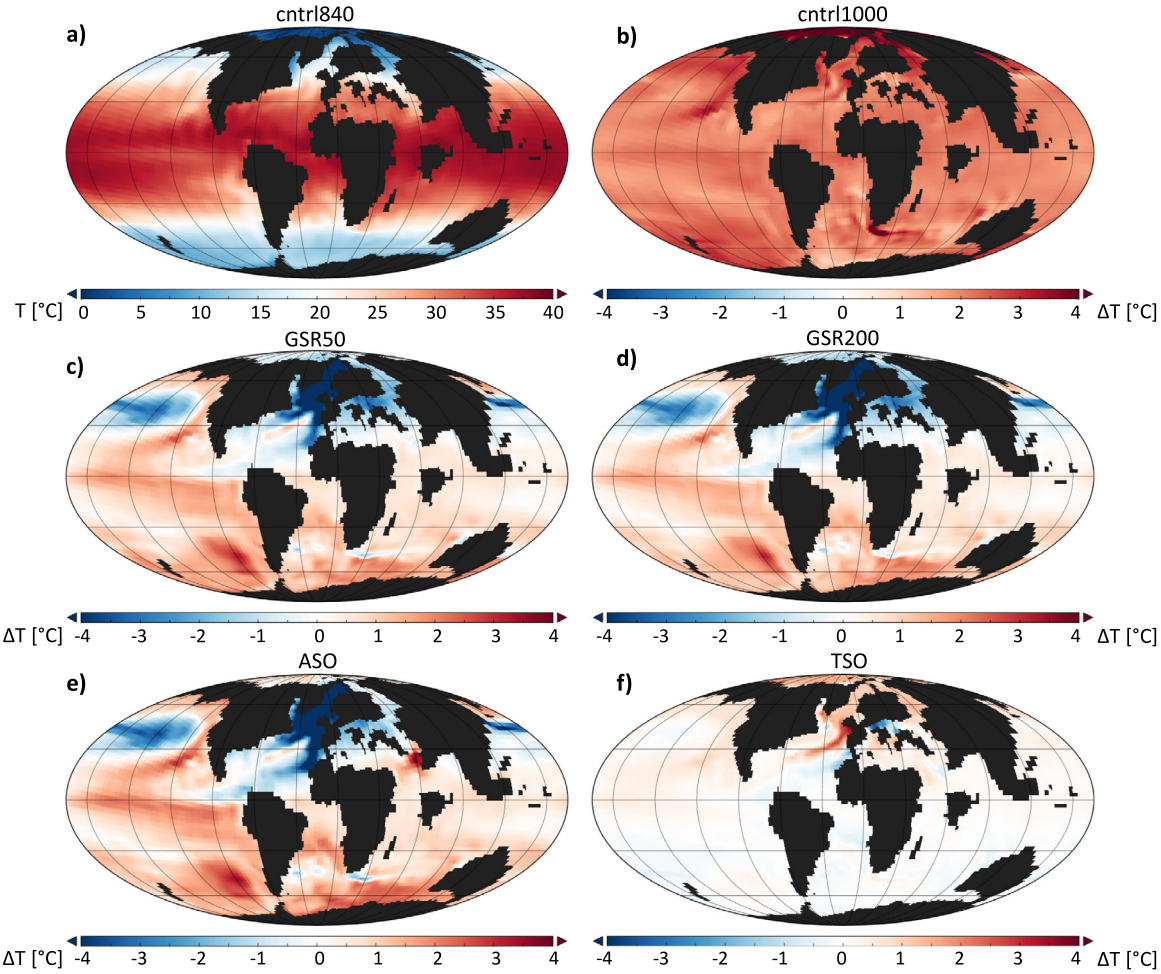


**Fig. 2. Annual Sea Surface Temperature (SST) for the middle Eocene simulations.** a) SST for *cntrl840*. ΔSST relative to *cntrl840* for b) *cntrl1000*, c) *GSR50*, d) *GSR200*, e) *ASO*, f) *TSO*.

ulated until year 7700. Two exceptions are the simulations *GSR200* and *cntrl1000*, which were simulated to year 9000 and 8800 respectively to allow for additional time for these simulations to equilibrate. To assess the steady state of our simulations, we calculated the linear regression of global mean surface and deep ocean temperatures for the last 700 years of each simulation. The maximum temperature drift was ∼0.01 °C/century for the surface ocean and ∼0.02 °C/century in the deep ocean. The last 100 years of each experiment were averaged for analysis.

## 3. Results

### 3.1. Global climate and ocean circulation

The global mean sea surface temperature (SST) in the Eocene *cntrl840* simulation is 27.8 °C. The mean SST in the tropics reaches 36.9 °C. The Arctic Ocean is characterized by the lowest annual SST of 1 to 3 °C, while the Southern Ocean is considerably warmer with 8 to 14 °C (Fig. 2a). Deep Ocean temperatures of ∼14 °C are very well in line with proxy records estimates for deep ocean temperature during the early–middle Eocene (Zachos et al., 2008). In our *cntrl1000* simulation global mean SST are 2.1 °C higher and reach 29.9 °C. The warming shows polar amplification, particularly in the Northern Hemisphere with changes of ∼4 °C in the Arctic, which is two times higher than the global average (Fig. 2b). The lowest SST change occurs at the location of Southern Component Water formation in the Weddell Sea.

Maximum SSS is reached in the Atlantic subtropical gyres due to high net evaporation (Fig. 3a). The lowest salinities occur in the Arctic as it is exposed to high net precipitation and only connected to the global oceans by the shallow Turgai Strait. Global SSS decreases by 0.4 psu with the 160 ppm increase in $CO_2$. Particularly the high latitudes are fresher, while the (sub-) equatorial Atlantic is slightly more saline under higher $CO_2$ concentration (Fig. 3b).

Bottom water ventilation occurs in the Weddell Sea and in the southern Nordic Seas (Fig. 4a), where sea surface densities are high. Here, surface waters are denser than intermediate waters, breaking the stratification of the water column during the winter season. Both locations are close to those of the modern deep-water formation sites, however their mixed layer depths (MLD) are much shallower compared to the modern ocean. Bottom water ventilation is strongly seasonal and occurs in the winter months of each Hemisphere. Ventilation in the Southern Ocean is reduced in the *cntrl1000* simulation, while the Northern Hemisphere MLD remains relatively constant (Fig. 4b). The sinking of water masses in the Nordic Seas leads to overflow of deep-water over the GSR into the North Atlantic and the establishment of a DWBC with annual average velocities of up to ∼14 cm/s in the western North Atlantic (Fig. 5a), fast enough to mobilize and redeposit fine grained sediments (McCave and Hall, 2006).

### 3.2. Model-data comparisons

Our *cntrl840* paleoclimate compares well with proxy-based paleotemperature estimates from the early–middle Eocene in the

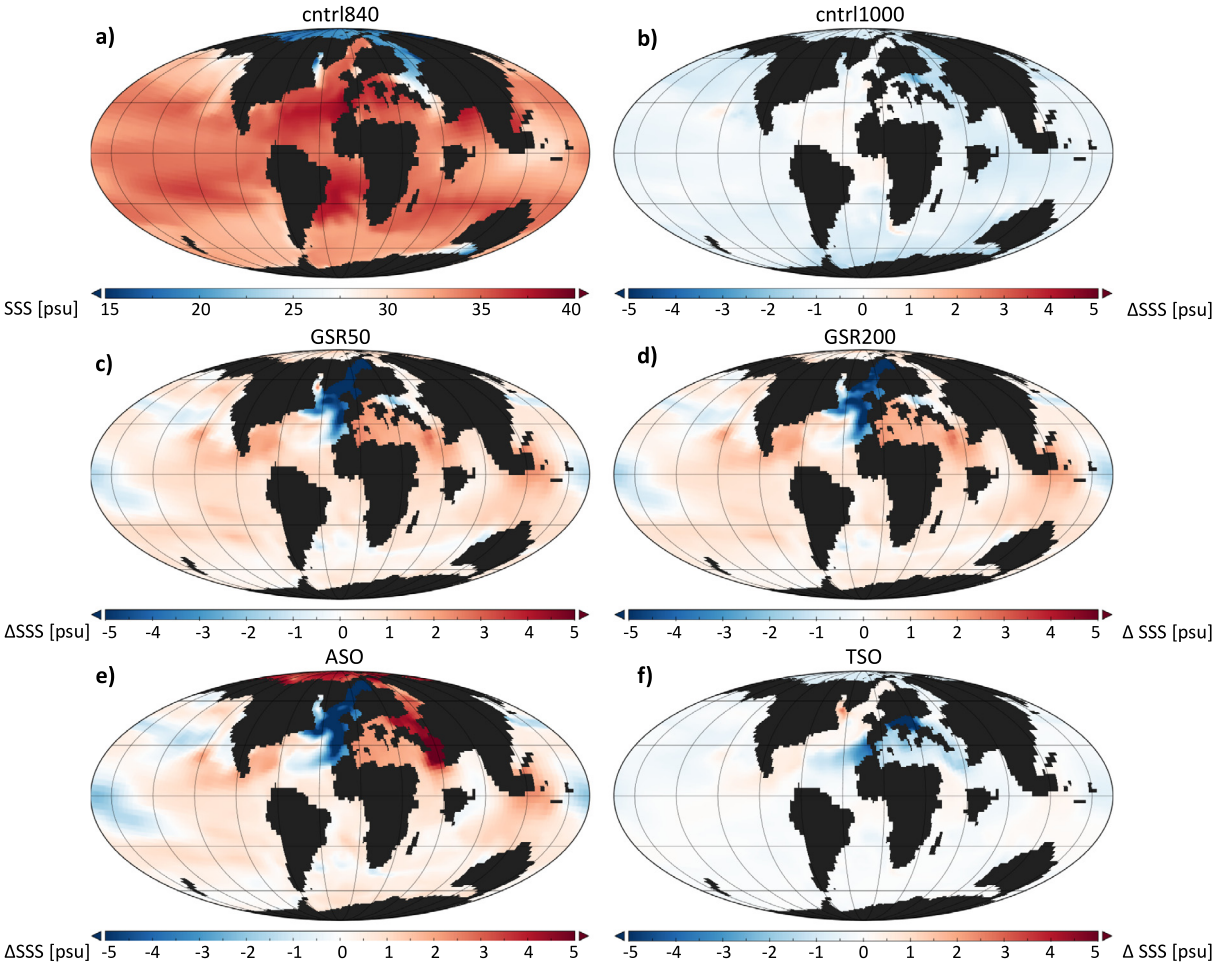


**Fig. 3. Annual Sea Surface Salinity (SSS) for the middle Eocene simulations.** a) SSS for *cntrl840*, ΔSSS relative to *cntrl840* for b) *cntrl1000*, c) *GSR50*, d) *GSR200*, e) *ASO*, f) *TSO*.

Southern Ocean between 45°S and 70°S and from the tropical Southern Hemisphere up to the Northern high latitudes between ca. 20°S and 70°N where 67% of the data points fall within the annual SAT envelope of our simulations (Fig. 6). However, in the Southern mid-latitudes between 25°S and 45°S a considerable discrepancy between proxy-derived and simulated temperatures exists, which exceeds 10 °C. The Arctic is the second area where simulated and proxy derived temperatures differ. Here, only 29% of the data points fall within the simulated temperature envelope while others are significantly higher than simulated temperatures. The inability to reproduce the high Arctic temperatures and the lower latitudinal temperature gradient observed in proxy data for the early Cenozoic is a common feature in studies simulating the extreme warmth of the Eocene, known as the "equable climate problem" (Huber and Caballero, 2011 and references therein). Southern Ocean SST is in very good agreement with proxies, while the discrepancy for Arctic SST is similar to those of other studies of greenhouse climate at ∼8 °C (e.g. Roberts et al., 2009). Various explanations for the data-model mismatch during greenhouse periods have been proposed. These include insufficient model sensitivity, misrepresentation of feedback mechanisms in climate models and seasonally biased proxy records at the high latitudes. Whether these discrepancies are related to model or proxy uncertainty is beyond the scope of this work, but has been discussed in detail by previous studies (e.g. Huber and Caballero, 2011). Nevertheless, proxy data around the deep-water formation sites in the Nordic Seas and the Southern Ocean fall within the temperature envelope of our simulations and thus allow us to evaluate ocean circulation.

### 3.3. Impacts of seaways on ocean circulation and climate

#### 3.3.1. Greenland–Scotland Ridge

The sill depth of the GSR in our experiments influences SST, SSS and density by regulating the inflow of warm, salty Atlantic surface waters into the Nordic Seas. Our experiments reflect the subsidence of the GSR from the early Eocene onwards. As a result of the GSR subsidence from 50 m to 200 m sill depth, annual SST above the GSR and in the Nordic Seas increase by up to 2 °C and SSS in the Nordic Seas increases by ∼5 psu (Fig. 2c and d). Further subsidence to 500 m sill depth enables intense inflow of warm salty water from the North Atlantic into the Nordic Seas and increases SST here by up to 7 °C and SSS by up to 6 psu (Fig. 2c and 3c). The greater inflow of warm, salty water from the North Atlantic causes sea surface density in the Nordic Seas to increase substantially with the sill depth of the GSR. As a result, the vertical density gradient in the Nordic Seas diminishes until it is small enough to allow for diapycnal mixing (Fig. 7). The deep Atlantic circulation is influenced as NCW overflows the GSR from the Nordic Seas and flows towards the North Atlantic increasing DWBC velocity (Fig. 5a, c, d). Our results suggest the threshold value in the GSR sill depth for NCW formation and the establishment of a DWBC lies between 200 and 500 m.

Our *GSR200* simulation is the only experiment in which the ocean circulation changes over the duration of the simulation. Before the collapse at simulation year 7600, the *GSR200* simulation was characterized by NCW formation in the Nordic Seas (Fig. 8a, b, c). This could indicate that *GSR200* is close to the threshold depth of the GSR sill that allows for NCW formation.

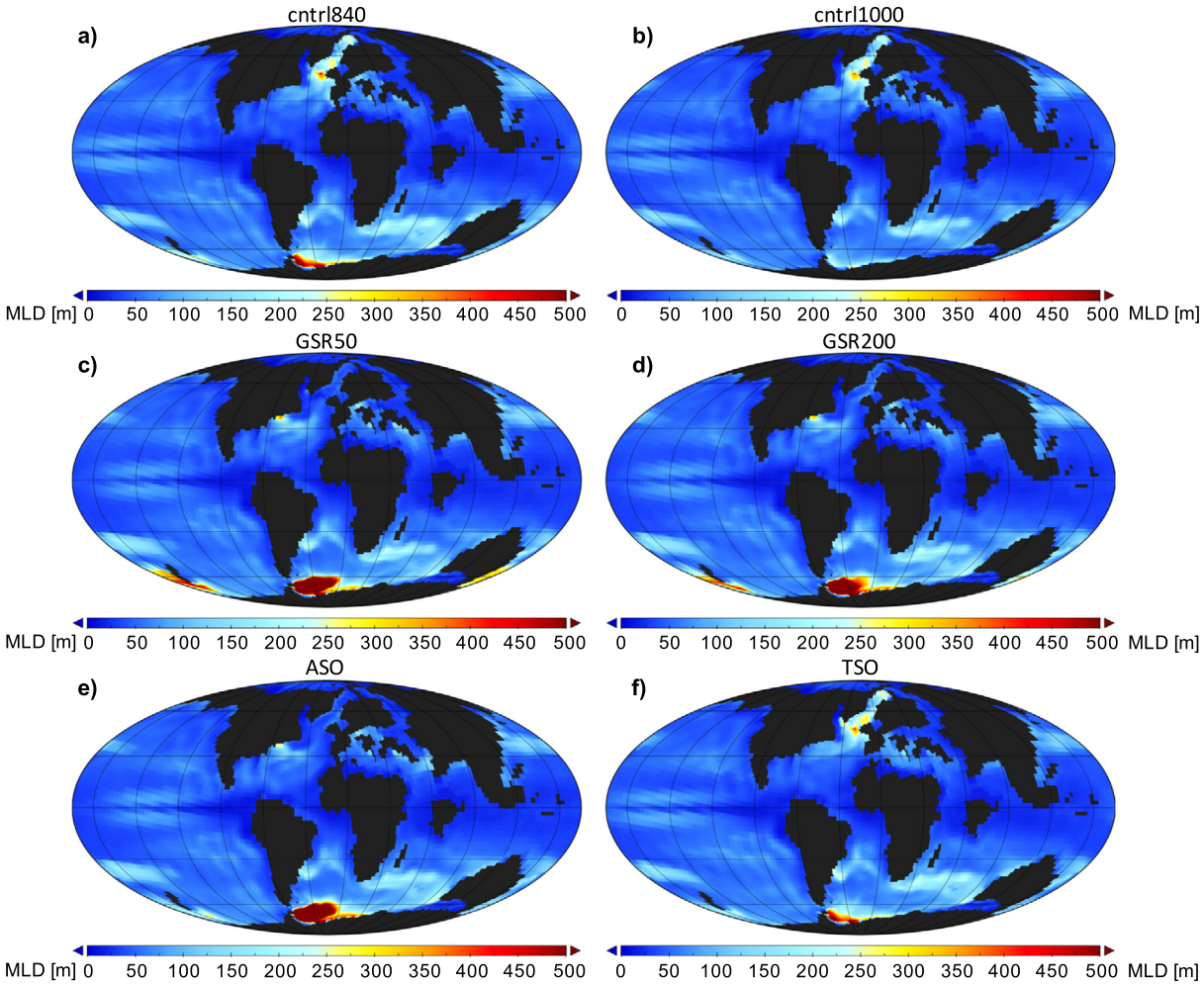


**Fig. 4. Annual mixed layer depth (MLD) for the middle Eocene simulations.** MLD for a) *cntrl840*, b) *cntrl1000*, c) *GSR50*, d) *GSR200*, e) *ASO*, f) *TSO*.

Furthermore, the collapse of the *GSR200* experiment allows us to evaluate the climatic influence of NCW in our simulations without changing any parameters. Here, global SST increase by 0.1 as the amount of deep water formation decreases and the North Atlantic cools considerably (by up to 7 °C) due to the collapse of NCW formation (Fig. 8d). Cooler Northern Hemisphere and warmer Southern Hemisphere SST are the result of the collapse in NCW formation.

### 3.3.2. Arctic seaway

The Arctic is ∼1 °C warmer in our *ASO* simulation compared to our *cntrl840* simulation, while the Nordic Seas cools by up to 10 °C. Most of the Southern Hemisphere SST increase by 1–3 °C while the northern mid-latitudes cool ∼1 °C in every ocean basin (Fig. 2e). Exchange between Arctic and North Atlantic waters results in saltier Arctic surface waters while the Nordic Seas and the North Atlantic are considerably freshened by the outflow of brackish waters from the Arctic by up to 10 psu (Fig. 3e). As a result, the sea surface density in the Nordic Seas decreases. The strong density gradient between the surface and underlying waters ($>1$ kg/m$^3$) prevents diapycnal mixing and mixed layer formation (Fig. 7). Therefore, the Weddell Sea remains the only site of deep-water formation. Here, MLD is increased by a factor of ∼2 due to the opening of the Arctic–North Atlantic connection (Fig. 4e). No DWBC flows along the western continental margin of the Atlantic (Fig. 5e).

### 3.3.3. Tethyan seaway

The Tethys is an enclosed basin in our *cntrl840* simulation and develops high SSS as it is situated in a climate zone characterized by high evaporation and low precipitation. Opening of the Tethys seaway (*TSO*) leads to the inflow of less saline tropical Indian Ocean waters into the Atlantic Ocean (Fig. 3f). Our *TSO* simulation shows Northern Hemisphere (particularly in the Nordic Seas and the Arctic) warming by 1 to 3 degrees, while the effect in the tropics and the Southern Hemisphere is relatively small (Fig. 2f). Increasing SSS is largely restricted to the western North Atlantic, the Nordic Sea and particularly the Labrador Sea. Our simulations do not show any sinking of WSDW in the Tethyan Ocean (Fig. 4f). While the Tethyan seaway does impact the heat and salt flux of the North Atlantic, the SST and SSS changes largely balance each other so that we do not observe a change in density (Fig. 7). Thus, the differences in mixed-layer depth in the Nordic Seas (Fig. 4f), and DWBC velocities in the North Atlantic in simulation *TSO* (Fig. 5f) are small compared to the *cntrl840* simulation.

## 4. Discussion

### 4.1. Greenland–Scotland Ridge

Our simulations identify the GSR sill depths as the major factor in the NCW formation in the Nordic Seas as it determines the rate of inflow of salty surface waters from the Atlantic into the Nordic Seas and it determines the rate of outflow of NCW into

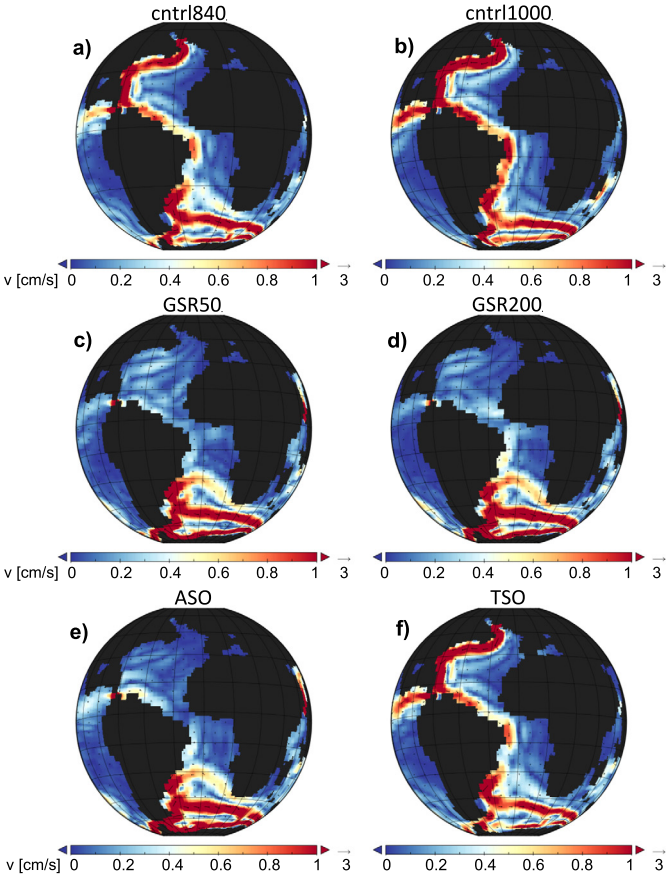


**Fig. 5. Atlantic Ocean current velocity at 1500 m water depth. Current velocity for** a) *cntrl840*, b) *cntrl1000*, c) *GSR50*, d) *GSR200*, e) *ASO*, f) *TSO*. DWBCs form in simulations a), b), and f), which are characterized by NCW formation.

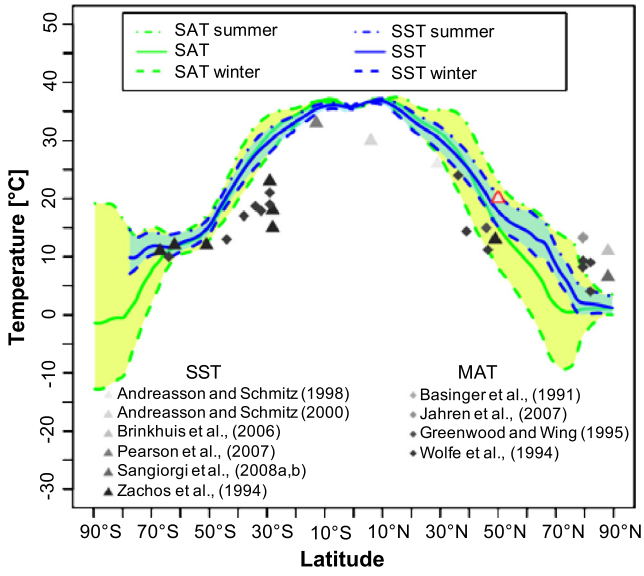


**Fig. 6. Data-model (cntrl840) comparison of surface air temperature (SAT) and sea surface temperature (SST) for the early–middle Eocene.** Gray triangles mark SST proxy data (Andreasson and Schmitz, 1998, 2000; Brinkhuis et al., 2006; Pearson et al., 2007; Sangiorgi et al., 2008a, 2008b; Zachos et al., 1994) and diamonds mark mean annual temperature (MAT) proxy data (Basinger, 1991; Greenwood and Wing, 1995; Jahren, 2007; Wolfe, 1994). The red triangle marks a proxy temperature estimate from the Nordic Seas (Andreasson and Schmitz, 2000).

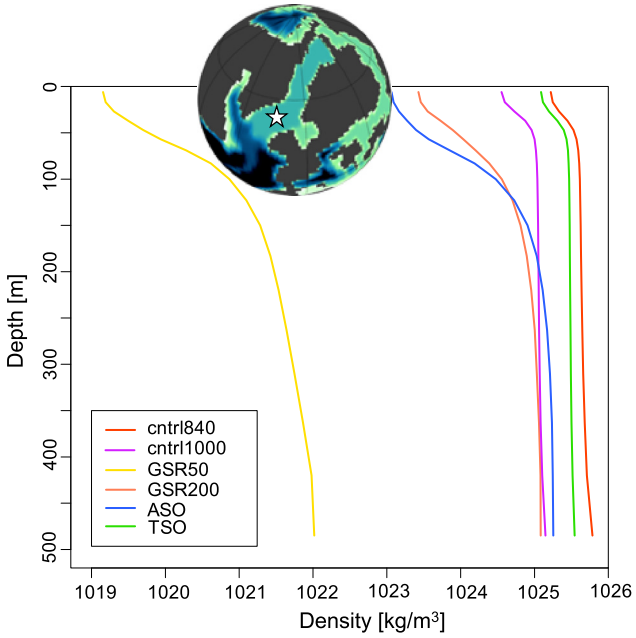


**Fig. 7. Annual density profiles of the southern Nordic Seas in the different simulations.** Colored lines indicate the density vs. depth for the six different simulations. The white star in the map marks the location of the profiles. Cntrl840, cntr1000 and TSO show no stratification of the water column during winter season.

the North Atlantic. Many studies have previously invoked a crucial role of the GSR sill depth in NCW formation and thus the onset of a bimodal AMOC (Poore et al., 2006; Stärz et al., 2017; Wright and Miller, 1996). Our results indicate that during the early–middle Eocene the threshold in the sill depth of the GSR for NCW formation was above 200 m. Stärz et al. (2017) found that bidirectional flow over the GSR is initiated between 30–80 m under Miocene boundary conditions. Defining the absolute depth of the GSR with uncertainties of less than 100 m has been proven difficult as it is dependent on several aspects including the subsidence history of the ridge, the mantle plume activity beneath Iceland (Parnell-Turner et al., 2014) and eustatic changes (Miller et al., 2005a). Today the difference between the deepest sections of the ridge and the average sill depth is ∼500 m. Thus, some parts of the ridge may have allowed significant overflow of deep-water, while other parts of the ridge were still subaerial. Parnell-Turner et al. (2014) show that during the early–middle Eocene, Iceland mantle plume activity was minimal. This could have caused the GSR sill depth to reach the threshold to allow for NCW formation at the onset of the Cenozoic cooling. We find that only simulations with NCW formation are characterized by DWBC that would explain the changes in North Atlantic sedimentation at the early–middle Eocene boundary.

### 4.2. Arctic seaway

The *ASO* simulation shows that even a very shallow connection with the Arctic Ocean allows for sufficient inflow of brackish water into the Nordic Seas to diminish deep-water formation here. In the *ASO* simulation, the Weddell Sea in the Atlantic sector of the Southern Ocean remains the only site of deep-water formation. This is in line with proxy evidence from the early Eocene, where this region was most likely the dominant deep-water source (e.g. Scher and Martin, 2004). Others propose deep water formation in the Ross Sea based on circulation models with a similar continental setup as our simulation *ASO* (Douglas et al., 2014). On the other hand, our results indicate that in a scenario without exchange with the Arctic Ocean (*cntrl840*), the Nordic Seas can

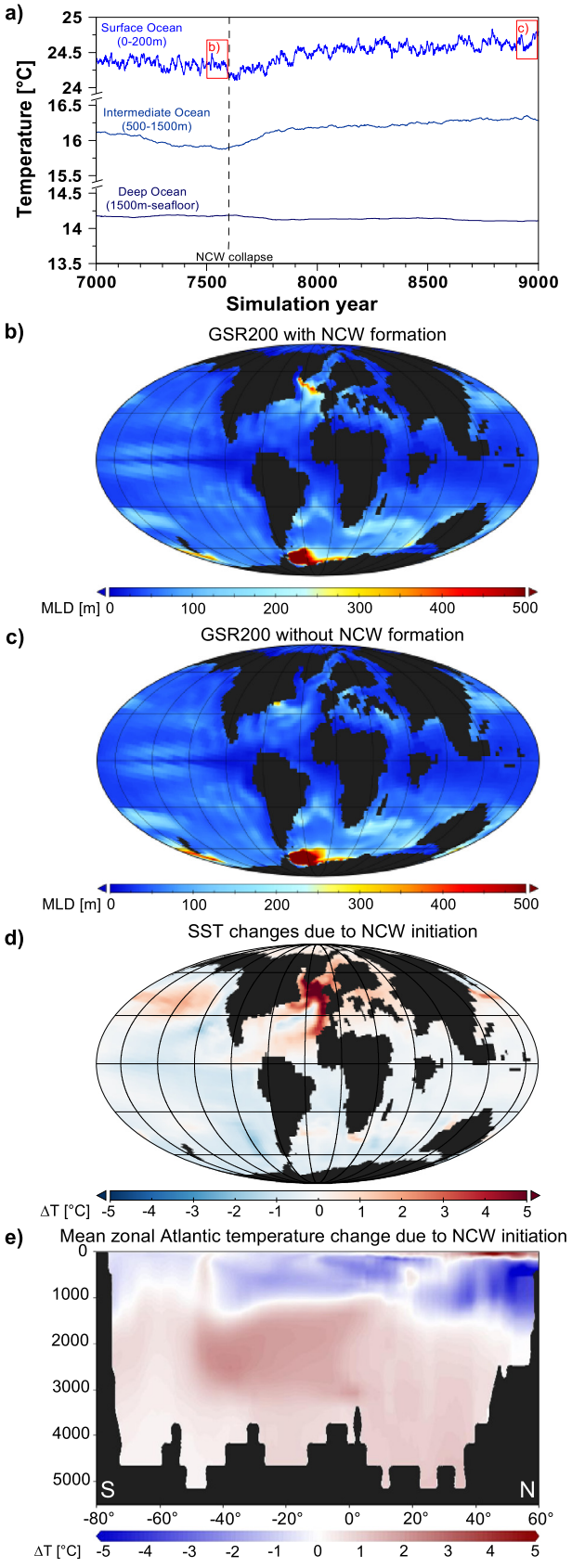


**Fig. 8. Climatic impacts of NCW formation in the *GSR200* simulation.** a) Ocean temperature timeseries. Intervals analyzed in b) and c) are marked by red squares, b) average annual MLD for model year 7500–7600 marked with a red square, c) average annual MLD for model year 8900–9000, d) ΔSST for time window b) relative to c), e) zonal mean temperature in the Atlantic for the time window b) relative to c).

sustain salinities high enough for deep-water formation. Indeed, a positive salt anomaly resulting from the very low SSS in the Arctic due to restriction of the seaways causing the onset of NCW formation has been previously identified (Roberts et al., 2009), while Cope and Winguth (2011) find no onset of NCW due to Arctic restrictions. These contrasting results may be caused by differences in sea surface density due to model sensitivity to greenhouse forcing.

Proxy records indicate lowest SSS resulting from the most severe restriction of Arctic seaways between 48.7 and 47.6 Ma (Waddell and Moore, 2008), which is supported by the deposition of the freshwater fern *Azolla* at this time (Barke et al., 2012; Brinkhuis et al., 2006). From 45 Ma onwards, exchange between the Arctic Ocean and the Nordic Seas likely became more frequent (Onodera et al., 2008). Rapid eustatic fluctuations up to 30 m (Miller et al., 2005a) may have periodically linked and separated Arctic surface waters with the Nordic Seas (Brinkhuis et al., 2006). The hampering effect of the brackish waters on NCW formation could have been balanced by the opening of the Drake Passage, as some climate models have shown that the NCW can be formed when the Arctic is connected to the Nordic Seas after the (proto-)ACC is established (Fyke et al., 2015). Thus, the changes in the Southern Ocean gateways (Bijl et al., 2013; Livermore et al., 2007) together with decreasing $CO_2$ concentrations (Anagnostou et al., 2016), the initiation of Northern Hemisphere sea ice (e.g. St. John, 2008; Stickley et al., 2009; Tripati et al., 2008), ongoing subsidence of the GSR and low Iceland mantle plume activity (Parnell-Turner et al., 2014) could have contributed to sustaining NCW formation and DWBCs after the flow of brackish Arctic surface waters into the Nordic Seas increased.

### 4.3. Tethyan seaway

Independent of the used paleogeographic setting, our simulations do not show the formation of WSDW in the Tethys as invoked by some studies for the early and middle Eocene (Pak and Miller, 1992; Scher and Martin, 2004). As a semi-enclosed basin in a high evaporation–low precipitation zone, the Tethys accumulates high SSS. Opening of the Tethys seaway on the other hand leads to the throughflow of less saline tropical Indian Ocean waters into the Atlantic Ocean (Fig. 7b). While parts of the surface waters pass through the Central American Seaway into the Pacific, another branch enters the Northern subtropical gyre, where high evaporation induces the transport of salty waters towards the Nordic Seas via the North Atlantic Current. Here, SST and SSS are enhanced due to the opening of the Tethys seaway. As the increase in SST and SSS in the Nordic Seas balance each other, the net effect on surface density here is small. MLD and DWBC velocities are slightly increased in the *TSO* simulation. The strengthening, but minor influence of Tethyan outflow is in agreement with simulations for the Miocene and modern Mediterranean outflow (Ivanovic et al., 2014a, 2014b). However, the response of the AMOC may depend on the position of the closure of the Tethyan seaway that determines the properties of Tethyan outflow. Closing the Tethyan Seaway further east can have a strongly enforcing effect on the AMOC (Butzin et al., 2011; Hamon et al., 2013).

### 4.4. Northern vs. Southern gateways

Our simulations demonstrate that changes in the heat and salt balance of the Nordic Seas caused by the tectonic evolution of the North Atlantic during the early–middle Eocene could have led to the onset of a bimodal AMOC without any gateway changes in the South Atlantic.

Toggweiler and Samuels (1993, 1995) attributed NCW formation to upwelling in the Southern Ocean but our results emphasize

the important role of the thermohaline balance of the North Atlantic and the vertical density gradients in the Nordic Seas. An important role of the North Atlantic in AMOC dynamics is in accordance with other studies highlighting the GSR sill depth (Poore et al., 2006; Wright and Miller, 1996) or the Arctic seaway restrictions (Roberts et al., 2009). Moreover, this finding is also supported by results from modeling studies that find no onset of NCW formation in response to the opening of Tasman Gateway (Sijp et al., 2011). Other studies found that the NCW formation initiates with the opening of the Drake Passage (Fyke et al., 2015). However, it should be noted that Sijp et al. (2011) and Fyke et al. (2015) both use paleoceanographic settings with a connection between the Arctic and the North Atlantic, which has a hampering effect on NCW formation. Furthermore, the response of the oceanic circulation to the opening of the Southern Ocean gateways, may depend on the climatic background state (Lefebvre et al., 2012). Thus, changes in the North Atlantic (e.g. Brinkhuis et al., 2006; Hohbein et al., 2012) and in the Southern Ocean (e.g. Bijl et al., 2013; Livermore et al., 2005) have the potential to drive the ocean circulation towards a modern-like bimodal state. Only the exact timing of the changes in these seaways will help to resolve the question, which changes led to the onset of NCW.

### 4.5. Interactions between climate and ocean circulation

In our simulations NCW formation transfers heat from the surface ocean towards the deep ocean.

Globally, the effects of the onset of NCW on surface temperatures are relatively small with a maximum SST change of 0.4 °C due to gateway changes. However, NCW formation can have a pronounced impact on regional temperatures. Minor global surface temperature effects that can be intensely amplified regionally are in agreement with results of Roberts et al. (2009) for Eocene NCW formation. The onset of NCW formation in our simulations (Fig. 8d, e) leads to Northern Hemisphere warming and Southern Hemisphere cooling, as the surface branch of the AMOC begins to transport heat towards the North Atlantic. Here, local temperatures are up to 7 °C higher when NCW formation is active. In other words, the onset of NCW formation during the early middle Eocene would have triggered pronounced surface warming in the North Atlantic. Bornemann et al. (2016) report no substantial cooling of the North Atlantic during the early middle Eocene, while Inglis et al. (2015) found a low SST gradient between the tropical and the northern Atlantic at this time. The onset of NCW provides a plausible mechanism that would mask the Eocene cooling in the North Atlantic by locally increasing temperatures due to enhanced heat transport from the tropics. Cooling occurs in the upper ~1000 m of the water column in the South Atlantic and in the subsurface in the Northern Hemisphere between about ~200–1500 m (Fig. 8e).

At the same time, the global deep ocean is warmed by the onset of NCW. Similarly to surface temperatures, changes in globally averaged deep ocean temperature in response to the onset of NCW are relatively small (maximum of 0.5 °C) compared to the changes arising from declining $CO_2$ around the early–middle Eocene. Consequently, they would likely have been dominated by changes in $CO_2$ over this interval that caused more pronounced global climatic changes (Anagnostou et al., 2016). This finding is in agreement with sensitivity studies attributing global climate change to $CO_2$ instead of changes in ocean circulation (e.g. DeConto and Pollard, 2003; Huber and Nof, 2006; Lunt et al., 2008).

The invigoration of a southward flowing DWBC that is indicated by North Atlantic contourite drift deposition (Boyle et al., 2017; Hohbein et al., 2012) and winnowing (Norris et al., 2001) can only be achieved in our model if NCW formation is active. Our results indicate that tectonic changes in gateway configuration could have contributed to the initiation of NCW and thus the invigoration of DWBC close to the early–middle Eocene boundary (Fig. 5). While $CO_2$ concentrations do play a role in the intensity and depth of overturning, changes in the North Atlantic Gateways connecting the North Atlantic with the Arctic via the Nordic Seas are the critical factor controlling the formation of NCW. Our experiments reveal how sensitive the global ocean circulation is to the thermohaline balance in the Nordic Seas. Very small changes in the depth and geometry of these ocean gateways may result in large-scale changes in ocean circulation and may thus have a profound impact on global climate and sedimentation patterns. Unfortunately, the exact timing and magnitude of such changes in seaway geometry remain difficult to reconstruct with direct geologic evidence. Therefore, improved tracer-based proxy reconstructions of the Eocene ocean circulation are necessary from North Atlantic and Arctic deep ocean sites to allow for paleoceanographic reconstructions providing indirect constraints on past ocean bathymetry. After NCW initiated through the subsidence of the sill below the discussed threshold, NCW formation intensity was a function of $CO_2$ concentration, variations in GSR sill depth and the Arctic seaways and of orbital forcing (Vahlenkamp et al., 2018). In other words, the development towards a bimodal AMOC was probably more irregular and transient than previously thought.

## 5. Conclusions

Simulations with the Earth System Model *COSMOS* reveal that large-scale changes in ocean circulation can result from minor changes (~200 m) in the depth of seaways connecting the Nordic Seas with the North Atlantic and the Arctic Ocean. The seaway between the North Atlantic and the Arctic must have been restricted in order to form NCW at the early–middle Eocene boundary. The GSR sill-depth must have reached a minimum depth of 200 m to allow for sufficient inflow of salty surface water into the Nordic Seas and to initiate sinking there. Our results thus indicate that changes in North Atlantic Ocean gateways alone could have been sufficient for deep-water formation in the North Atlantic and for the invigoration of early–middle Eocene DWBC under favorable astronomical forcing. Our simulations do not show any WSDW formation and the influence of outflow of Tethyan waters towards the Atlantic on NCW formation in our simulations is minor. After the onset of NCW a combination of further gateway development and climatic factors such as the drawdown of atmospheric $CO_2$ concentrations and astronomical forcing would have determined the intensity of NCW formation.

## Acknowledgements

M.V., D.D.V. and H.P. are funded by European Research Council Consolidator Grant EarthSequencing (grant agreement 617462). I.N. is funded by the National Center of Science, Poland (DEC-2012/07/N/ST10/03419) and the DAAD. I.N. gratefully acknowledges G. Knorr (AWI) and J. Tyszka (ING PAN) for their scientific support. G.L. is funded by the Helmholtz Association through the PACES and REKLIM programs (grant PACEST3WP2). The authors thank Appy Sluijs and two anonymous reviewers for their constructive comments that greatly improved this manuscript.

## Appendix A. Supplementary material

Supplementary material related to this article can be found online at https://doi.org/10.1016/j.epsl.2018.06.031.

## References

Anagnostou, E., John, E.H., Edgar, K.M., Foster, G.L., Ridgwell, A., Inglis, G.N., Pancost, R.D., Lunt, D.J., Pearson, P.N., 2016. Changing atmospheric $CO_2$ concentration was the primary driver of early Cenozoic climate. Nature 533, 380–384.

Andreasson, F.P., Schmitz, B., 1998. Tropical Atlantic seasonal dynamics in the early middle Eocene from stable oxygen and carbon isotope profiles of mollusk shells. Paleoceanography 13, 183–192.
Andreasson, F.P., Schmitz, B., 2000. Temperature seasonality in the early middle Eocene North Atlantic region: evidence from stable isotope profiles of marine gastropod shells. Geol. Soc. Am. Bull. 112, 628–640.
Backman, J., Moran, K., McInroy, D.B., Mayer, L., 2006. Arctic Coring Expedition (ACEX): Paleoceanographic and Tectonic Evolution of the Central Arctic Ocean.
Barke, J., van der Burgh, J., van Konijnenburg-van Cittert, J.H.A., Collinson, M.E., Pearce, M.A., Bujak, J., Heilmann-Clausen, C., Speelman, E.N., van Kempen, M.M.L., Reichart, G.-J., Lotter, A.F., Brinkhuis, H., 2012. Coeval Eocene blooms of the freshwater fern Azolla in and around Arctic and Nordic seas. Palaeogeogr. Palaeoclimatol. Palaeoecol. 337–338, 108–119.
Barker, P.F., 2001. Scotia Sea regional tectonic evolution: implications for mantle flow and palaeocirculation. Earth-Sci. Rev. 55, 1–39.
Basinger, J., 1991. The fossil forests of the Buchanan Lake Formation (early Tertiary), Axel Heiberg Island, Canadian Arctic Archipelago: preliminary floristics and paleoclimate. Bull., Geol. Surv. Can., 39–65.
Berggren, W., Schnitker, D., 1983. Cenozoic marine environments in the North Atlantic and Norwegian–Greenland Sea. In: Structure and Development of the Greenland–Scotland Ridge. Springer, pp. 495–548.
Berggren, W.A., 1982. Role of ocean gateways in climatic change. In: Climate in Earth History, pp. 118–125.
Berggren, W.A., Hollister, C., 1977. Plate tectonics and paleocirculation – commotion in the ocean. Tectonophysics 38, 11–48.
Bijl, P.K., Bendle, J.A., Bohaty, S.M., Pross, J., Schouten, S., Tauxe, L., Stickley, C.E., McKay, R.M., Röhl, U., Olney, M., 2013. Eocene cooling linked to early flow across the Tasmanian Gateway. Proc. Natl. Acad. Sci. USA 110, 9645–9650.
Bornemann, A., D'haenens, S., Norris, R.D., Speijer, R.P., 2016. The demise of the early Eocene greenhouse – decoupled deep and surface water cooling in the eastern North Atlantic. Glob. Planet. Change 145, 130–140.
Borrelli, C., Cramer, B.S., Katz, M.E., 2014. Bipolar Atlantic deepwater circulation in the middle-late Eocene: effects of Southern Ocean gateway openings. Paleoceanography 29, 308–327.
Boyle, P.R., Romans, B.W., Tucholke, B.E., Norris, R.D., Swift, S.A., Sexton, P.F., 2017. Cenozoic North Atlantic deep circulation history recorded in contourite drifts, offshore Newfoundland, Canada. Mar. Geol. 385, 185–203.
Brinkhuis, H., Schouten, S., Collinson, M.E., Sluijs, A., Damsté, J.S.S., Dickens, G.R., Huber, M., Cronin, T.M., Onodera, J., Takahashi, K., 2006. Episodic fresh surface waters in the Eocene Arctic Ocean. Nature 441, 606–609.
Butzin, M., Lohmann, G., Bickert, T., 2011. Miocene ocean circulation inferred from marine carbon cycle modeling combined with benthic isotope records. Paleoceanography 26.
Cope, J.T., Winguth, A., 2011. On the sensitivity of ocean circulation to arctic freshwater input during the Paleocene/Eocene Thermal Maximum. Palaeogeogr. Palaeoclimatol. Palaeoecol. 306, 82–94.
Coxall, H.K., Huck, C.E., Huber, M., Lear, C.H., Legarda-Lisarri, A., O'Regan, M., Sliwinska, K.K., van de Flierdt, T., de Boer, A.M., Zachos, J.C., Backman, J., 2018. Export of nutrient rich Northern component water preceded early Oligocene Antarctic glaciation. Nat. Geosci. 11, 190–196.
Cramer, B., Toggweiler, J., Wright, J., Katz, M., Miller, K., 2009. Ocean overturning since the Late Cretaceous: inferences from a new benthic foraminiferal isotope compilation. Paleoceanography 24.
Davies, R., Cartwright, J., Pike, J., Line, C., 2001. Early Oligocene initiation of North Atlantic deep water formation. Nature 410, 917–920.
DeConto, R.M., Pollard, D., 2003. Rapid Cenozoic glaciation of Antarctica induced by declining atmospheric $CO_2$. Nature 421, 245–249.
Douglas, P.M., Affek, H.P., Ivany, L.C., Houben, A.J., Sijp, W.P., Sluijs, A., Schouten, S., Pagani, M., 2014. Pronounced zonal heterogeneity in Eocene southern high-latitude sea surface temperatures. Proc. Natl. Acad. Sci. USA 111, 6582–6587.
Elsworth, G., Galbraith, E., Halverson, G., Yang, S., 2017. Enhanced weathering and $CO_2$ drawdown caused by latest Eocene strengthening of the Atlantic meridional overturning circulation. Nat. Geosci. 10, 213.
Exon, N., Kennett, J., Malone, M., Brinkhuis, H., Chaproniere, G., Ennyu, A., Fothergill, P., Fuller, M., Grauert, M., Hill, P., 2002. Drilling reveals climatic consequences of Tasmanian Gateway opening. Eos, Trans. Am. Geophys. Union 83, 253–259.
Franks, P.J., Royer, D.L., Beerling, D.J., Van de Water, P.K., Cantrill, D.J., Barbour, M.M., Berry, J.A., 2014. New constraints on atmospheric $CO_2$ concentration for the Phanerozoic. Geophys. Res. Lett. 41, 4685–4694.
Fricke, H.C., Wing, S.L., 2004. Oxygen isotope and paleobotanical estimates of temperature and $\delta^{18}$O-latitude gradients over North America during the early Eocene. Am. J. Sci. 304, 612–635.
Fyke, J.G., D'Orgeville, M., Weaver, A.J., 2015. Drake Passage and Central American Seaway controls on the distribution of the oceanic carbon reservoir. Glob. Planet. Change 128, 72–82.
Gierz, P., Lohmann, G., Wei, W., 2015. Response of Atlantic overturning to future warming in a coupled atmosphere–ocean–ice sheet model. Geophys. Res. Lett. 42, 6811–6818.
Gleason, J.D., Thomas, D.J., Moore, T.C., Blum, J.D., Owen, R.M., Haley, B.A., 2009. Early to middle Eocene history of the Arctic Ocean from Nd–Sr isotopes in fossil fish debris, Lomonosov Ridge. Paleoceanography 24 (2).
Gough, D., 1981. Solar interior structure and luminosity variations. In: Physics of Solar Variations. Springer, pp. 21–34.
Greenwood, D.R., Wing, S.L., 1995. Eocene continental climates and latitudinal temperature gradients. Geology 23, 1044–1048.
Hagemann, S., Dümenil, L., 1997. A parametrization of the lateral waterflow for the global scale. Clim. Dyn. 14, 17–31.
Hamon, N., Sepulchre, P., Lefebvre, V., Ramstein, G., 2013. The role of eastern Tethys seaway closure in the Middle Miocene Climatic Transition (ca. 14 Ma). Clim. Past 9, 2687–2702.
Hibler III, W., 1979. A dynamic thermodynamic sea ice model. J. Phys. Oceanogr. 9, 815–846.
Hohbein, M.W., Sexton, P.F., Cartwright, J.A., 2012. Onset of North Atlantic Deep Water production coincident with inception of the Cenozoic global cooling trend. Geology 40, 255–258.
Huber, M., Caballero, R., 2011. The early Eocene equable climate problem revisited. Clim. Past 7, 603.
Huber, M., Nof, D., 2006. The ocean circulation in the southern hemisphere and its climatic impacts in the Eocene. Palaeogeogr. Palaeoclimatol. Palaeoecol. 231, 9–28.
Huber, M., Sloan, L.C., 2001. Heat transport, deep waters, and thermal gradients: coupled simulation of an Eocene greenhouse climate. Geophys. Res. Lett. 28, 3481–3484.
Hulsbos, R., Kroon, D., Jansen, H., Van Hinte, J., 1989. Lower Eocene benthic foraminifera and paleoenvironment of the outer Vöring Plateau, Norwegian Sea (DSDP Site 338). Micropaleontology, 256–273.
Inglis, G.N., Farnsworth, A., Lunt, D., Foster, G.L., Hollis, C.J., Pagani, M., Jardine, P.E., Pearson, P.N., Markwick, P., Galsworthy, A.M., 2015. Descent toward the Icehouse: Eocene sea surface cooling inferred from GDGT distributions. Paleoceanography 30, 1000–1020.
Ivanovic, R., Valdes, P., Flecker, R., Gutjahr, M., 2014a. Modelling global-scale climate impacts of the late Miocene Messinian Salinity Crisis. Clim. Past 10, 607–622.
Ivanovic, R.F., Valdes, P.J., Gregoire, L., Flecker, R., Gutjahr, M., 2014b. Sensitivity of modern climate to the presence, strength and salinity of Mediterranean–Atlantic exchange in a global general circulation model. Clim. Dyn. 42, 859–877.
Jagniecki, E.A., Lowenstein, T.K., Jenkins, D.M., Demicco, R.V., 2015. Eocene atmospheric $CO_2$ from the nahcolite proxy. Geology 43, 1075–1078.
Jahren, A.H., 2007. The Arctic forest of the middle Eocene. Annu. Rev. Earth Planet. Sci. 35, 509–540.
Jakobsson, M., Backman, J., Rudels, B., Nycander, J., Frank, M., Mayer, L., Jokat, W., Sangiorgi, F., O'Regan, M., Brinkhuis, H., 2007. The early Miocene onset of a ventilated circulation regime in the Arctic Ocean. Nature 447, 986–990.
Jungclaus, J., Keenlyside, N., Botzet, M., Haak, H., Luo, J.-J., Latif, M., Marotzke, J., Mikolajewicz, U., Roeckner, E., 2006. Ocean circulation and tropical variability in the coupled model ECHAM5/MPI-OM. J. Climate 19, 3952–3972.
Kennett, J.P., 1977. Cenozoic evolution of Antarctic glaciation, the circum-Antarctic Ocean, and their impact on global paleoceanography. J. Geophys. Res. 82, 3843–3860.
Knorr, G., Butzin, M., Micheels, A., Lohmann, G., 2011. A warm Miocene climate at low atmospheric $CO_2$ levels. Geophys. Res. Lett. 38.
Langton, S.J., Rabideaux, N.M., Borrelli, C., Katz, M.E., 2016. Southeastern Atlantic deep-water evolution during the late-middle Eocene to earliest Oligocene (Ocean Drilling Program Site 1263 and Deep Sea Drilling Project Site 366). Geosphere 12, 1032–1047.
Lawver, L.A., Gahagan, L.M., 2003. Evolution of Cenozoic seaways in the circum-Antarctic region. Palaeogeogr. Palaeoclimatol. Palaeoecol. 198, 11–37.
Lefebvre, V., Donnadieu, Y., Sepulchre, P., Swingedouw, D., Zhang, Z.S., 2012. Deciphering the role of southern gateways and carbon dioxide on the onset of the Antarctic Circumpolar Current. Paleoceanography 27.
Livermore, R., Hillenbrand, C.-D., Meredith, M., Eagles, G., 2007. Drake Passage and Cenozoic climate: an open and shut case? Geochem. Geophys. Geosyst. 8.
Livermore, R., Nankivell, A., Eagles, G., Morris, P., 2005. Paleogene opening of Drake passage. Earth Planet. Sci. Lett. 236, 459–470.
Lott, F., Miller, M.J., 1997. A new subgrid-scale orographic drag parametrization: its formulation and testing. Q. J. R. Meteorol. Soc. 123, 101–127.
Lunt, D.J., Foster, G.L., O'Brien, C.L., Pancost, R.D., Robinson, S.A., 2016. Palaeogeographic controls on climate and proxy interpretation. Clim. Past 12, 1181.
Lunt, D.J., Valdes, P.J., Haywood, A., Rutt, I.C., 2008. Closure of the Panama Seaway during the Pliocene: implications for climate and Northern Hemisphere glaciation. Clim. Dyn. 30, 1–18.
Marsland, S.J., Haak, H., Jungclaus, J.H., Latif, M., Röske, F., 2003. The Max-Planck-Institute global ocean/sea ice model with orthogonal curvilinear coordinates. Ocean Model. 5, 91–127.
McCave, I.N., Hall, I.R., 2006. Size sorting in marine muds: processes, pitfalls, and prospects for paleoflow-speed proxies. Geochem. Geophys. Geosyst. 7.
Miller, K.G., Fairbanks, R.G., Mountain, G.S., 1987. Tertiary oxygen isotope synthesis, sea level history, and continental margin erosion. Paleoceanography 2, 1–19.
Miller, K.G., Kominz, M.A., Browning, J.V., Wright, J.D., Mountain, G.S., Katz, M.E., Sugarman, P.J., Cramer, B.S., Christie-Blick, N., Pekar, S.F., 2005a. The Phanerozoic record of global sea-level change. Science 310, 1293–1298.
Miller, K.G., Wright, J.D., Browning, J.V., 2005b. Visions of ice sheets in a greenhouse world. Mar. Geol. 217, 215–231.

Mosar, J., Eide, E.A., Osmundsen, P.T., Sommaruga, A., Torsvik, T.H., 2002. Greenland–Norway separation: a geodynamic model for the North Atlantic. Norwegian J. Geol., 282.
Mountain, G.S., Miller, K.G., 1992. Seismic and geologic evidence for early Paleogene deepwater circulation in the western North Atlantic. Paleoceanography 7, 423–439.
Nielsen, S.G., Mar-Gerrison, S., Gannoun, A., LaRowe, D., Klemm, V., Halliday, A.N., Burton, K.W., Hein, J.R., 2009. Thallium isotope evidence for a permanent increase in marine organic carbon export in the early Eocene. Earth Planet. Sci. Lett. 278, 297–307.
Norris, R.D., Kroon, D., Huber, B.T., Erbacher, J., 2001. Cretaceous–Palaeogene ocean and climate change in the subtropical North Atlantic. Geol. Soc. (Lond.) Spec. Publ. 183, 1–22.
Oberhänsli, H., Müller-Merz, E., Oberhänsli, R., 1991. Eocene paleoceanographic evolution at 20–30 S in the Atlantic Ocean. Palaeogeogr. Palaeoclimatol. Palaeoecol. 83, 173–215.
Onodera, J., Takahashi, K., Jordan, R.W., 2008. Eocene silicoflagellate and ebridian paleoceanography in the central Arctic Ocean. Paleoceanography 23.
Pak, D.K., Miller, K.G., 1992. Paleocene to Eocene benthic foraminiferal isotopes and assemblages: implications for deepwater circulation. Paleoceanography 7, 405–422.
Parnell-Turner, R., White, N., Henstock, T., Murton, B., Maclennan, J., Jones, S.M., 2014. A continuous 55-million-year record of transient mantle plume activity beneath Iceland. Nat. Geosci. 7, 914–919.
Pearson, P.N., van Dongen, B.E., Nicholas, C.J., Pancost, R.D., Schouten, S., Singano, J.M., Wade, B.S., 2007. Stable warm tropical climate through the Eocene Epoch. Geology 35, 211–214.
Poore, H., Samworth, R., White, N., Jones, S., McCave, I., 2006. Neogene overflow of Northern Component Water at the Greenland–Scotland Ridge. Geochem. Geophys. Geosyst. 7.
Roberts, C.D., LeGrande, A.N., Tripati, A.K., 2009. Climate sensitivity to Arctic seaway restriction during the early Paleogene. Earth Planet. Sci. Lett. 286, 576–585.
Roeckner, E., Bäuml, G., Bonaventura, L., Brokopf, R., Esch, M., Giorgetta, M., Hagemann, S., Kirchner, I., Kornblueh, L., Manzini, E., 2003. The Atmospheric General Circulation Model ECHAM 5, Part I: Model Description.
Sangiorgi, F., Brumsack, H.J., Willard, D.A., Schouten, S., Stickley, C.E., O'Regan, M., Reichart, G.J., Sinninghe Damsté, J.S., Brinkhuis, H., 2008a. A 26 million year gap in the central Arctic record at the greenhouse–icehouse transition: looking for clues. Paleoceanography 23.
Sangiorgi, F., van Soelen, E.E., Spofforth, D.J., Pälike, H., Stickley, C.E., St. John, K., Koç, N., Schouten, S., Sinninghe Damsté, J.S., Brinkhuis, H., 2008b. Cyclicity in the middle Eocene central Arctic Ocean sediment record: orbital forcing and environmental response. Paleoceanography 23.
Scher, H.D., Martin, E.E., 2004. Circulation in the Southern Ocean during the Paleogene inferred from neodymium isotopes. Earth Planet. Sci. Lett. 228, 391–405.
Scher, H.D., Martin, E.E., 2006. Timing and climatic consequences of the opening of Drake Passage. Science 312, 428–430.
Schettino, A., Turco, E., 2011. Tectonic history of the western Tethys since the Late Triassic. Geol. Soc. Am. Bull. 123, 89–105.
Sewall, J.v., Van De Wal, R., Van Der Zwan, K., Van Oosterhout, C., Dijkstra, H., Scotese, C., 2007. Climate model boundary conditions for four Cretaceous time slices. Clim. Past 3, 647–657.
Sexton, P.F., Wilson, P.A., Norris, R.D., 2006. Testing the Cenozoic multisite composite $\delta^{18}$O and $\delta^{13}$C curves: new monospecific Eocene records from a single locality, Demerara Rise (Ocean Drilling Program Leg 207). Paleoceanography 21.
Sijp, W.P., England, M.H., Huber, M., 2011. Effect of the deepening of the Tasman Gateway on the global ocean. Paleoceanography 26.
Speelman, E.N., Sewall, J.O., Noone, D., Huber, M., von der Heydt, A., Damsté, J.S., Reichart, G.-J., 2010. Modeling the influence of a reduced equator-to-pole sea surface temperature gradient on the distribution of water isotopes in the Early/Middle Eocene. Earth Planet. Sci. Lett. 298, 57–65.
Speelman, E.N., van Kempen, M.M., Barke, J., Brinkhuis, H., Reichart, G.-J., Smolders, A.J., Roelofs, J.G., Sangiorgi, F., de Leeuw, J.W., Lotter, A.F., 2009. The Eocene Arctic Azolla bloom: environmental conditions, productivity and carbon drawdown. Geobiology 7, 155–170.
St. John, K., 2008. Cenozoic ice-rafting history of the central Arctic Ocean: terrigenous sands on the Lomonosov Ridge. Paleoceanography 23, PA1S05.
Stampfli, G.M., Borel, G.D., 2004. The TRANSMED transects in space and time: constraints on the paleotectonic evolution of the Mediterranean domain. In: The TRANSMED Atlas. The Mediterranean Region from Crust to Mantle. Springer, pp. 53–80.
Stampfli, G.M., Hochard, C., 2009. Plate tectonics of the Alpine realm. Geol. Soc. (Lond.) Spec. Publ. 327, 89–111.
Stärz, M., Jokat, W., Knorr, G., Lohmann, G., 2017. Threshold in North Atlantic–Arctic Ocean circulation controlled by the subsidence of the Greenland–Scotland Ridge. Nat. Commun. 8, 15681.
Stickley, C.E., Brinkhuis, H., Schellenberg, S.A., Sluijs, A., Röhl, U., Fuller, M., Grauert, M., Huber, M., Warnaar, J., Williams, G.L., 2004. Timing and nature of the deepening of the Tasmanian Gateway. Paleoceanography 19.
Stickley, C.E., St. John, K., Koç, N., Jordan, R.W., Passchier, S., Pearce, R.B., Kearns, L.E., 2009. Evidence for middle Eocene Arctic sea ice from diatoms and ice-rafted debris. Nature 460, 376–379.
Thiede, J., Eldholm, O., 1983. Speculations about the paleodepth of the Greenland–Scotland Ridge during late Mesozoic and Cenozoic times. In: Structure and Development of the Greenland–Scotland Ridge. Springer, pp. 445–456.
Thomas, D.J., Bralower, T.J., Jones, C.E., 2003. Neodymium isotopic reconstruction of late Paleocene–early Eocene thermohaline circulation. Earth Planet. Sci. Lett. 209, 309–322.
Toggweiler, J., Samuels, B., 1993. Is the magnitude of the deep outflow from the Atlantic Ocean actually governed by Southern Hemisphere winds? In: The Global Carbon Cycle. Springer, pp. 303–331.
Toggweiler, J., Samuels, B., 1995. Effect of Drake Passage on the global thermohaline circulation. Deep-Sea Res., Part 1, Oceanogr. Res. Pap. 42, 477–500.
Tripati, A.K., Eagle, R.A., Morton, A., Dowdeswell, J.A., Atkinson, K.L., Bahé, Y., Dawber, C.F., Khadun, E., Shaw, R.M., Shorttle, O., 2008. Evidence for glaciation in the Northern Hemisphere back to 44 Ma from ice-rafted debris in the Greenland Sea. Earth Planet. Sci. Lett. 265, 112–122.
Vahlenkamp, M., Niezgodzki, I., De Vleeschouwer, D., Bickert, T., Harper, D., Kirtland Turner, S., Lohmann, G., Sexton, P., Zachos, J., Pälike, H., 2018. Astronomically paced changes in deep-water circulation in the western North Atlantic during the middle Eocene. Earth Planet. Sci. Lett. 484, 329–340.
Via, R.K., Thomas, D.J., 2006. Evolution of Atlantic thermohaline circulation: early Oligocene onset of deep-water production in the North Atlantic. Geology 34, 441–444.
Waddell, L.M., Moore, T.C., 2008. Salinity of the Eocene Arctic Ocean from oxygen isotope analysis of fish bone carbonate. Paleoceanography 23.
Wing, S.L., 2003. Causes and Consequences of Globally Warm Climates in the Early Paleogene. Geological Society of America.
Wolfe, J.A., 1994. Tertiary climatic changes at middle latitudes of western North America. Palaeogeogr. Palaeoclimatol. Palaeoecol. 108, 195–205.
Wright, J.D., Miller, K.G., 1996. Control of North Atlantic deep water circulation by the Greenland–Scotland Ridge. Paleoceanography 11, 157–170.
Zachos, J., Pagani, M., Sloan, L., Thomas, E., Billups, K., 2001. Trends, rhythms, and aberrations in global climate 65 Ma to present. Science 292, 686–693.
Zachos, J.C., Dickens, G.R., Zeebe, R.E., 2008. An early Cenozoic perspective on greenhouse warming and carbon-cycle dynamics. Nature 451, 279–283.
Zachos, J.C., Stott, L.D., Lohmann, K.C., 1994. Evolution of early Cenozoic marine temperatures. Paleoceanography 9, 353–387.
Zhang, Z., Nisancioglu, K.H., Flatøy, F., Bentsen, M., Bethke, I., Wang, H., 2011. Tropical seaways played a more important role than high latitude seaways in Cenozoic cooling. Clim. Past 7, 801–813.
Ziegler, P.A., 1988. Evolution of the Arctic–North Atlantic and the Western Tethys: a visual presentation of a series of Paleogeographic–Paleotectonic maps. AAPG Mem. 43, 164–196.